PCCP

PAPER

View Article Online
View Journal | View Issue

Cite this: *Phys. Chem. Chem. Phys.*, 2025, **27**, 8540

Charge and length dependent build-up of environment sensitive lamellin β-peptides†

Sohini Chakraborty,‡[ad] Kamal el Battioui,‡[ab] Tasvilla Sonallya,[ab] Imola Cs. Szigyártó,[a] Kata Horváti,[c] Zoltán Varga,[ae] Tünde Juhász[a] and Tamás Beke-Somfai*[a]

Received 2nd December 2024,
Accepted 28th March 2025

DOI: 10.1039/d4cp04561k

rsc.li/pccp

Supramolecular constructs of peptides with their unique morphologies and biomimetic nature exhibit immense potential in developing functional biomaterials. β-Peptides are imperative in this respect due to their propensity to form proteolytically stable, diverse and structurally well-defined assemblies. Our recent investigations focused on the assembly patterns of neutral heterochiral acyclic β^3-peptide sequences which showed enhanced antibacterial activity upon introduction of positively charged side chains. These sequences adopt a lamellar morphology in phosphate rich media, hence are termed lamellins. Notably, slight sequential modifications also resulted in changes in assembly formation. Thus, to better understand their properties, four peptides have been synthesized with gradually increasing cationic nature and length varied between hexa- and octapeptides, while preserving the hydrophobic N-terminal and the alternating chirality along the backbone. The effect of charge and length on the morphology and supramolecular organization of these sequences in high-salt phosphate conditions (PBS) and low ionic strength water were systematically investigated. With an increase in charge, the affinity for assembly formation increased in PBS and decreased in water. The octapeptides exhibited a higher affinity for ordered assembly formation when compared to the hexapeptides as demonstrated in their unique CD spectral pattern, suggesting altered chirality at the supramolecular level. In the presence of liposomes, a more homogenous conformational distribution was observed in PBS media, with the large assemblies of the octapeptides retaining their molecular conformation. Hemolysis assays demonstrated that minor sequence modifications could result in an order of magnitude difference in activity. Thus, through selective modifications of the peptide backbone, novel supramolecules can be engineered with tailored morphology, physicochemical and membrane characteristics, which can be used for targeted biological applications.

Introduction

Supramolecular peptide self-assembling systems which can be optimized with respect to their three-dimensional properties and structure have potential applicability in manipulating fundamental biomedical processes.[1–5] Typically, these assembled edifices have distinct hydrophilic and hydrophobic regions which are held together with the help of non-covalent interactions such as hydrogen bonds, electrostatic interactions, van der Waals interactions, hydrophobic interactions and π–π overlap.[6–9] These functional assemblies are highly tunable and are triggered by the external environment such as the salt content of the media, pH, temperature, *etc.* They have future potential in widespread applications ranging from multifunctional scaffolds for tissue engineering and regenerative medicine,[10] to antibiotic treatments against drug resistance pathogens[11] and biocompatible solutions in wearable electronics.[12–14] Due to the dynamic and reversible nature of these interactions, the overall supramolecular arrangement of these assemblies can be easily modified to obtain different architectures such as nanofibers, micelles, vesicles, nanorods, nanoribbons or nanosheets.[15]

[a] *Institute of Materials and Environmental Chemistry, HUN-REN Research Centre for Natural Sciences, Budapest H-1117, Hungary. E-mail: beke-somfai.tamas@ttk.hu*
[b] *Hevesy György PhD School of Chemistry, Eötvös Loránd University, Budapest H-1117, Hungary*
[c] *MTA-HUN-REN TTK "Momentum" Peptide-Based Vaccines Research Group, Institute of Materials and Environmental Chemistry, HUN-REN Research Centre for Natural Sciences, Budapest H-1117, Hungary*
[d] *Innovation & Translational Research Hub (iTRH), Department of Chemistry, Presidency University, Bengaluru 560064, Karnataka, India*
[e] *Department of Physical Chemistry and Materials Science, Budapest University of Technology and Economics, Műegyetem rkp. 3, Budapest 1111, Hungary*

† Electronic supplementary information (ESI) available. See DOI: https://doi.org/10.1039/d4cp04561k

‡ These authors contributed equally to this work.

Besides natural peptides, β-peptides have garnered increased research impetus owing to their proteolytic stability[16] as well as their propensity to form higher order complex assemblies.[17–20] They differ from natural α-peptides in the presence of an additional methylene group between the peptide bonds and can be denoted as β^2- or β^3-depending on the position of residue side chain in their backbone.[21] Additionally, their secondary structures can be highly optimized by altering the nature of their side-chain and chirality.[22,23] Amongst these, β^3-peptides have been extensively investigated owing to their ease of synthesis[24] along with their ability to adopt diverse structures similar to proteins such as helices, hairpins, sheets and distinct quaternary folds.[18,25–29] Furthermore, their extended backbone offers more access to three-dimensional space which is usually inaccessible to natural peptides resulting in the possibility of more complex architectures, mimicking the intricate structures found in natural proteins. However, owing to the additional backbone methylene group, β^3-peptides with homochiral amino acids lack the same alternating positioning of the side chains along the peptide backbone which natural, or α-peptides and proteins have as an intrinsic property. This difference is of importance for making oligomers where more extended secondary structures are dominant, leading to assemblies where intermolecular hydrogen bonds appear similarly to those in amyloid structures.[30] Note, that such, primarily helical, β-peptides have already been explored to some extent for their antimicrobial applicability. For example, Degrado *et al.*[25,26] and Arvidsson *et al.*[27] reported β^3-peptides containing the repeating triad β^3-Ala-β^3Lys-β^3X (where X = Val or Phe). These peptides self-assembled into an amphiphilic trifaced 3_{14} helical structure and displayed potent antimicrobial activity towards both Gram-negative and positive bacteria. Similarly, Gellman *et al.*[31] reported β^3-peptides composed of cyclic APC ((3*S*,4*R*)-*trans*-3-aminopyrrolidine-4-carboxylic acid) and ACPC ((*R*,*R*)-*trans*-2-aminocyclopentanecarboxylic acid) which formed 12-helical structures with strong antimicrobial properties inspired from magainins.[32] Seebach *et al.* and Arvidsson *et al.* also developed β-peptides composed of alternating β^2- and β^3-amino acids that folded into 10/12-helices which were highly active, especially against Gram-positive bacteria.[33] Although non-helical β-AMPs are less explored, Mosca *et al.* focused on the design of amphiphilic cationic β^{3R3}-peptides, that adopted a secondary structure similar to β-sheet which exhibited antimicrobial activity, particularly against Gram-positive bacteria.[34] Along these lines, since most of the reported works focused on β-peptides which adopted helical conformations, we initially developed zig-zag β^3-peptides, with acyclic amino acids having alternating chirality in the backbone.[35,36] These species, depending on the sequence, could form small oligomers, or longer lamellar morphologies, thus termed lamellins. Our primary investigations focused on the design of a zwitterionic scaffold, and its specific alteration towards antibacterial use, by introducing multiple cationic charges. However, considering the diverse potential applicability of their controlled self- and co-assembling capacity, a detailed understanding is essential, based on subtle, stepwise modifications.

Therefore, in the present study, we compare short lamellin β^3-peptide sequences with slight changes in their backbone to increase gradually their cationic nature. Also, as the arrangement into a lamellar structure is expected to be dependent on sequence length, we also analyze how length variation affects formed morphologies. We performed biophysical characterizations on these systems and studied their conformational and assembly preferences also as a function of the surrounding environment, *i.e.* in water, in physiological-like buffer composition, as well as in the presence of lipid bilayers. Finally, to assess their potential toxicity, hemolytic assays were performed.

Results and discussion

Design and peptide selection

For several cationic antimicrobial peptides (AMPs), it has been established that the antimicrobial activity is dependent primarily on their structure.[37,38] The appropriate balance between charge and hydrophobic residues promotes the initial electrostatic attraction to the negatively charged bacterial membrane to exert rapid bactericidal action. Based on these insights, similar systems were designed which could allow well-separated hydrophobic and hydrophilic residues mimicking these natural systems.[25,27,31] Related, our earlier studies focused on a group of β^3-hexapeptides[35] which was initially developed and investigated for its oligomerization affinity and its membrane activity. For these peptides, the N-terminus was maintained as hydrophobic to enforce membrane activity, whereas the remaining residues were alternated in chirality. A water-soluble β^3-hexapeptide sequence composed of a leucine rich hydrophobic core and a hydrophilic surface with a single glutamate and lysine side-chain, with alternating side chain chirality and a total of 0 charge was used as a scaffold (peptide 5 in Szigyártó *et al.*,[35] here termed peptide EK). The heterochiral pattern ensured a non-helical conformation and thus the peptide could easily self-assemble into oligomeric bundles in water,[35] while in some conditions can also form large lamellar assemblies (Szigyártó *et al.*, 2025, submitted). Recently we have introduced further alterations to EK that lead to supramolecular assemblies with antimicrobial activity that is triggered by the outer surface of bacterial membranes[36] (Table 1).

To understand how to construct similar antimicrobial assemblies in a systematic manner, we identified that their charge dependence would be beneficial to address, especially in changing environments. Based on the properties of the neutral EK,[35] we extrapolated towards increased charge, while keeping the alternating side chain chirality. For gradually increased charge, the combination of glutamates (E) and lysines (K) was altered, thus selecting the following four peptides for the current study: EK (charge 0), EKK (charge +1), 2K (charge +2), and 3K (charge +3). In case of EKK and 3K, an additional lysine was added to the zwitterionic hexapeptides, however, to avoid potential structural effects due to K being the terminal residue, these sequences have an additional terminal hydrophobic residue that also preserves the ability to form an apolar inner

Table 1 Chemical structure of the peptides used in this study. EK (hexamer, charge 0), EKK (octamer, charge +1), 2K (hexamer, charge +2) and 3K (octamer, charge +3) with the hydrophobic leucines and valines marked in black, anionic glutamates in red and cationic lysines in blue

Peptide	Net charge	Sequence
EK	0	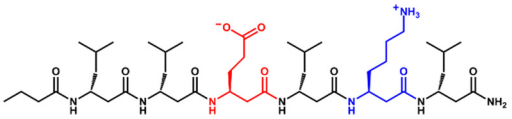 but-β-(3*R*)-Leu-β-(3*R*)-Leu-β-(3*S*)-Glu-β-(3*R*)-Leu-β-(3*S*)-Lys-β-(3*R*)-Leu-NH_2
EKK	+1	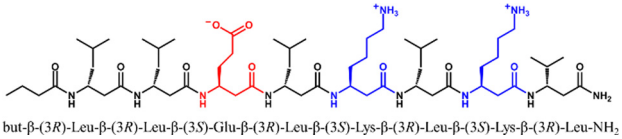 but-β-(3*R*)-Leu-β-(3*R*)-Leu-β-(3*S*)-Glu-β-(3*R*)-Leu-β-(3*S*)-Lys-β-(3*R*)-Leu-β-(3*S*)-Lys-β-(3*R*)-Leu-NH_2
2K	+2	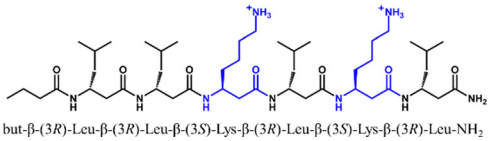 but-β-(3*R*)-Leu-β-(3*R*)-Leu-β-(3*S*)-Lys-β-(3*R*)-Leu-β-(3*S*)-Lys-β-(3*R*)-Leu-NH_2
3K	+3	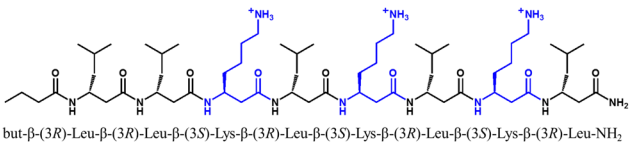 but-β-(3*R*)-Leu-β-(3*R*)-Leu-β-(3*S*)-Lys-β-(3*R*)-Leu-β-(3*S*)-Lys-β-(3*R*)-Leu-β-(3*S*)-Lys-β-(3*R*)-Leu-NH_2

core during oligomerization, and thus EKK and 3K are octameric. Note that as hydrophobic residue our primary choice was leucine, however in the case of EKK this residue caused synthetic problems, probably due to uncontrolled aggregation, therefore it was substituted to a valine instead at the C-terminal position. These four selected peptides were then submitted to a detailed biophysical comparison addressing conformational diversity, dominant supramolecular morphologies, and membrane affinity in different environments (Table 1).

Conformational diversity in various environments

The conformational state of the freshly dissolved peptides was tested in water and in high salt phosphate PBS using circular dichroism (CD) spectroscopy. Secondary structures of β-peptides are still challenging to analyze as similar CD spectral patterns are often produced for different secondary structures.[39,40] However, the relative changes in CD spectra give valuable and reliable information.[41] Relying on our recent studies on lamellins, as well as the support of other techniques, such as dynamic light scattering (DLS), and infrared spectroscopy (IR), we aimed to interpret the relative changes of CD spectra here.[35,36] In water, most of the peptides exhibited a spectral pattern of rather low intensity peaks at ~210 nm, which is compatible with a random coil conformation. As an exception, EK resembles an assembled lamellin state[36] (Fig. 1(a)) based on a characteristic strong minimum at 206 nm, similar to that obtained for *cis*-ACPC β-peptides with an elongated strand-like conformation.[42] In PBS, the hexameric EK retains a random or strand-like conformation (Fig. 1(b)), while 2K shows a lamellin-type CD pattern (Fig. 1(b)), which closely resembles that of EK in pure water (Fig. 1(a)). In contrast, the intense positive signals at ~205 nm observed for the octameric EKK and 3K could be attributed to the formation of larger morphologies as observed earlier[36] and could be considered analogous to natural amyloid fibrils.[43]

The conformational diversities were further assessed using attenuated total reflection-Fourier transform infrared (ATR-FTIR or IR) spectroscopy. The amide I band at 1600–1700 cm^{-1} represents mainly the C=O vibration in peptide bonds while the amide II band in the range of 1500–1600 cm^{-1} depicts the N–H bending vibrations of the peptide backbone which are observed not only for natural peptides and proteins but also for non-natural ones.[44,45] These specific regions can be sensitive to the secondary structure of the individual peptides, and also to the assembled state, and the protonated state of some side chain groups.[46] At both high and low ionic strength, an amide I band centered at ~1650 cm^{-1} is prominent for all the four peptides suggesting the predominance of an elongated, preferentially strand-like structure. Moreover, stronger and weaker shoulders at ~1680 cm^{-1} and ~1635 cm^{-1} are also observed, likely due to a non-hydrogen-bonded or turn population and intermolecular H-bonding, respectively (Fig. 1(c)).[35,44,47] Note that in water, the shoulder at ~1680 cm^{-1} gradually builds up as the charge of the peptides increases, suggesting that this band component could be related to the Lys side chains. In PBS, this shoulder is less intense but clearly present for all three net cationic peptides, further supporting that this band is linked to peptide charge (Fig. 1(d)). The shoulder at ~1620 cm^{-1} is more pronounced in PBS than in water, suggesting higher tendency to form H-bonded fibrillar morphologies, which is in line with CD results above. Additionally, two amide II band components detected at ~1560 cm^{-1} and ~1574 cm^{-1} for both EK and EKK in water are likely indicative of salt-bridge formation between glutamate and lysine side chains.[48–50]

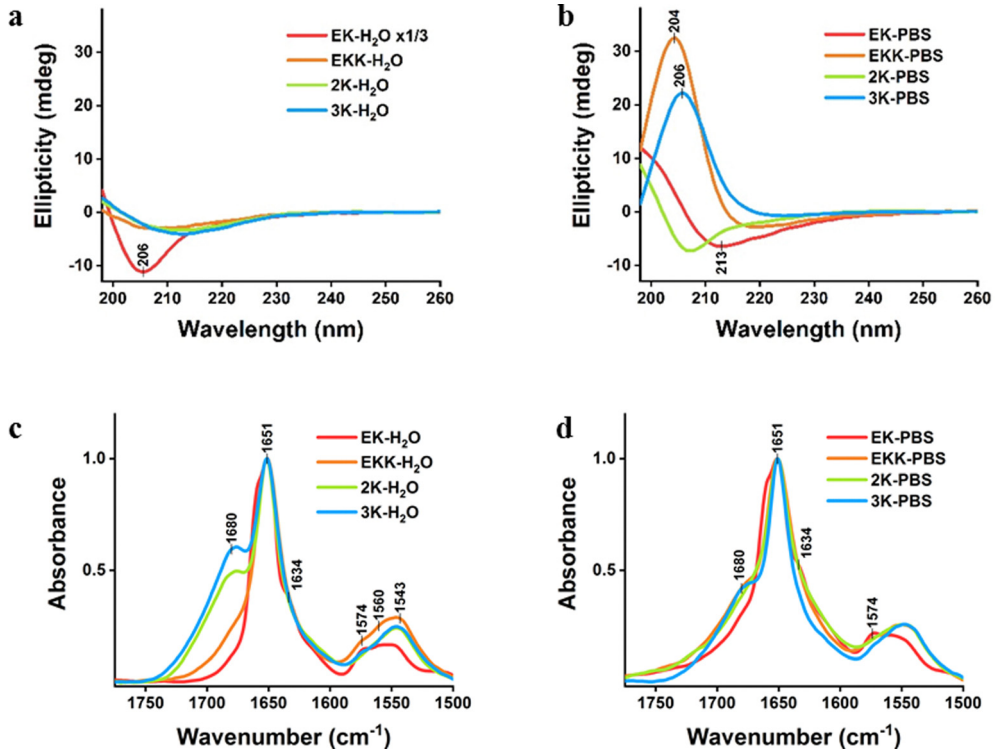

Fig. 1 Circular dichroism of the peptides at a concentration of 125 μM were recorded in various media, (a) in H_2O (pH = 6.5), note that EK-H_2O was multiplied by a factor 1/3, (b) in PBS (10 mM, pH 7.4) at 25 °C. A broad negative peak with a minimum is observed for all the four peptides in water pointing towards a random coil/extended structure, whereas in PBS, the hexameric EK and 2K retain their CD signature while the octameric EKK and 3K display the appearance of a strong positive maximum at ~205 nm, suggesting the formation of ordered assemblies. The representative CD in this figure has been illustrated from at least three independent measurements. ATR-IR spectra of the peptides (125 μM) (c) in water, (d) in PBS. In the absence of any other counter ion, *i.e.*, in water media, this band at ~1680 cm^{-1} is more intense. Additionally, the intensity of the band increases with charge, pointing towards a plausible neutralization effect of these H-bonds.

Assembly formation

To obtain a better view on size distribution of the peptide assemblies, dynamic light scattering (DLS) was used. The detected particle sizes suggested assembly formation for all peptide variants in both water and PBS, though to different extents (ESI,† Fig. S8 and Table S2). For EKK and 2K, a single dominant population with a diameter in the high nanometer range can be detected. Notably, for EK and 3K in water, two populations of comparable intensity were obtained, which suggests that there is an apparent equilibrium between at least two types of assemblies with different sizes.

The assemblies were also tested for their binding capacity to the fluorescent probe ANS (1-anilinonaphthalene-8-sulfonate).[51] ANS interaction[52] can be used to characterize surface hydrophobicity, and aggregation/fibrillation.[53] Assuming that significant ANS binding capacity is expected only for peptide associates, in particularly if exposing hydrophobic patches and nearby positive charges, the ANS fluorescence could be correlated with assembly formation. In water, the peptides bearing Glu, *i.e.* EK and EKK, showed remarkable ANS binding. (ESI,† Fig. S1). In comparison, in phosphate-rich media, EK showed lower ANS binding, however, higher ANS intensities were observed with all net charged peptides, suggesting that PBS could promote assembly formation for the charged variants (ESI,† Fig. S1). Particularly, the octa peptides, EKK and 3K, display higher ANS binding than the corresponding hexapeptides, EK and 2K.

To gain detailed information on the morphology of the assemblies, transmission electron microscopy (TEM) images were collected. In water, the extra two residues in EKK rendered more elongated ribbon-like fibrillar morphology to the octapeptide (Fig. 2(c), Fig. S3, S7 and Table S1, ESI†) compared to shorter fibrillar constructs of the hexameric EK (Fig. 2(a), Fig. S7 and Table S1, ESI†). In contrast, the more cationic peptides 2K and 3K presented less sophisticated architectures but more amorphous spherical associates (Fig. 2(e), (g) and Fig. S6a, ESI†). In PBS, for EK and EKK, more arranged rectangular lamellae was observed (Fig. 2(b), (d), Fig. S2, S4, S7 and Table S1, ESI†) which resembled lamellin-3K in terms of shape[36] (Fig. 2(f), (h), Fig. S5, S6b, S7 and Table S1, ESI†).

For all the four peptides, the formed lamellae shared a consistent striped pattern likely arising from the alternating chirality of the repetitive β-(3*R*)-Leu-β-(3*S*)-Lys motifs which leads to an amphiphilic zig-zag conformation and promotes phosphate-assisted co-assembly formation.[36] The bright stripes of the lamellae result from the Leu-rich hydrophobic peptide regions[54] while the darker ones could be assigned to the hydrophilic layers arranged between the PBS phosphate ions and the lysine side chains of the peptides. Distinct changes in

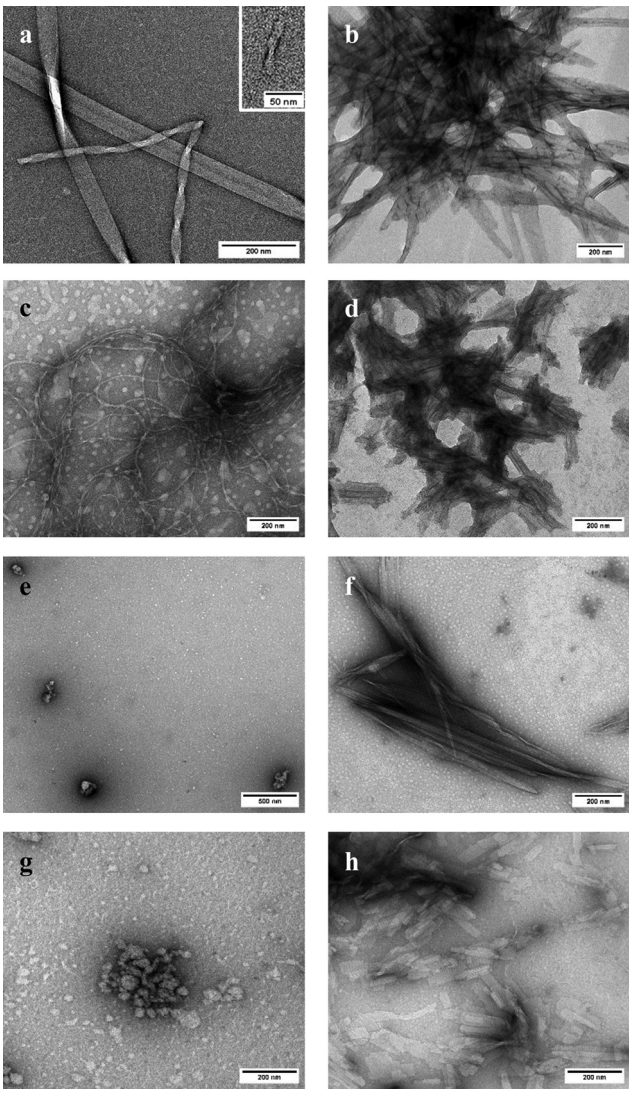

Fig. 2 Electron micrograph images of peptides showing morphology diversity in different media. EK (a) in water, twisted fibrils and shorter rod-like (inset) assemblies can be observed, (b) in PBS, striped lamellar morphology is displayed. EKK (c) in water, elongated fibrils are noticed, (d) in PBS, more packed and striped rectangular lamellae are present. 2K (e) in water, presence of spherical associates, (f) in PBS, fibrils or lamellin-2K can be identified. 3K (g) in water, presence of aggregates, (h) in PBS, lamellar pleated sheet also known as lamellin-3K. Peptide concentration was 125 μM.

morphology observed here reiterate the role of the positive charged groups in ordered lamellae formation. It should be noted for EK that besides longer fibrils, the increased presence of smaller oligomeric assemblies identified earlier,[35] could also be observed here, which suggests an equilibrium between diverse assemblies under these conditions (Fig. 2(a)). The co-presence of smaller and larger assemblies in water is clearly supported by DLS data showing either two distinct populations in water or a large increase in polydispersity with dominating micrometer size particles in PBS (Fig. S8 and Table S2, ESI†). It is worth noting here that the formation of extended lamellar or fibrillar morphologies closely correlated with the elevated ANS fluorescence values (Fig. S1, ESI†).

Interactions with lipid membranes

Formation of these assemblies was further investigated in lipid environment, modelling biological membranes with the use of liposomes. Model vesicles composed of DOPC (1,2-dioleoyl-*sn-glycero*-3-phosphocholine, PC), a zwitterionic phospholipid, and a combined zwitterionic and anionic DOPC/DOPG (1,2-dioleoyl-*sn-glycero*-3-[phospho-*rac*-(1-glycerol)], PC/PG, ratio 4 : 1) lipids were used. Note, that for these measurements, solutions of the peptides prepared in water or PBS were added in an order of magnitude excess to liposome solutions prepared in PBS, as for lipid systems a limited salt content is necessary for stability. To monitor assembly formation, CD spectra recorded in the presence of liposomes are compared to those taken without the lipids.

PC vesicles in water. Among the four peptides, EK-H_2O with PC (EK-H_2O-PC), displayed the most prominent spectral changes in their CD spectrum with a maximum at ~201 nm. Very similar changes were observed also for 3K in water, (3K-H_2O-PC) exhibiting a maximum at 203 nm similar to the characteristic peak of 3K-PBS (Fig. 3(a) and (d)). In contrast, for EKK-H_2O-PC and 2K-H_2O-PC, only minor changes were observed in the CD spectra (Fig. 3(b) and (c)).

PC/PG vesicles in water. EKK-H_2O-PC/PG and 3K-H_2O-PC/PG show a very similar spectrum, with a narrow and well-defined minimum at 208 nm, similar to that of EK in water. (Fig. 3(a), (b) and (d)). EK-H_2O-PC/PG presents the same CD spectral change as EK-H_2O-PC implying no degree of liposome specificity (Fig. 3(a)).

PC vesicles in PBS. EK-PBS-PC, EKK-PBS-PC and 3K-PBS-PC systems seem to result in similar CD spectra as in the lamellar morphologies of 3K-PBS[36] with a maximum at ~205 nm (Fig. 3(a), (b) and (d)).

PC/PG vesicles in PBS. EK exhibits a similar spectral behaviour with PC/PG and PC liposomes as in water though the intensities are lower (Fig. 3(a)). EK-PBS-PC/PG and EKK-PBS-PC/PG behave comparably to their homologues in PC, nevertheless, the relative positioning of these high intensity signals is somewhat shifted compared to that of 3K-PBS. The octapeptides EKK and 3K suggest that PBS induces the formation of lamellar assemblies, and the liposomes have a minor effect on the secondary structures of the formed morphology (Fig. 3(b) and (d)).

Interestingly, 2K displays the lowest response towards the various lipid systems in changing environments,[30,53] as the CD signals of 2K in water are not affected significantly by the liposomes and in PBS, only a slight decrease in intensity is observed (Fig. 3(c)).

Besides initial detailed characterization by CD, to reach an overview on the interactions between the peptides and lipid bilayers, we also addressed these systems using IR spectroscopy (Fig. S9–S12, ESI†). The deeper insertion of the peptides into the lipid membrane can be studied by following the shift in the methylene vibrations.[55,56] It was interesting to note that, in presence of PC/PG liposomes in water, upon addition of the peptides, the CH_2 stretching bands of lipid acyl chains experience a shift suggesting a perturbation of the lipid packing/order in the membranes. Furthermore, it is also apparent, that in PBS, those peptides which form lamellae, do not significantly

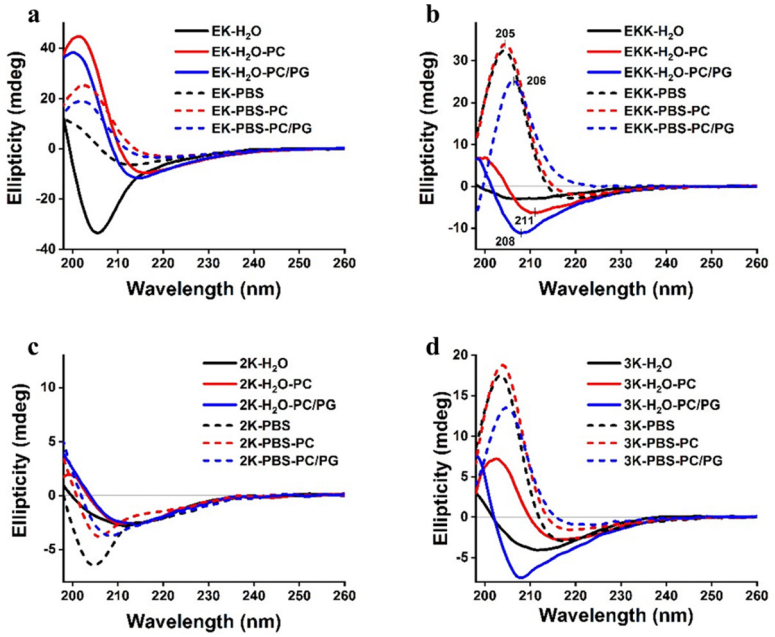

Fig. 3 CD spectra of peptides in presence of liposome in water and in PBS, for (a) EK, (b) EKK, (c) 2K and (d) 3K. EK in both water and PBS exhibits a CD spectral pattern, characterized by a maximum at ~205 nm with varying intensities, similar to those obtained for the lamellins previously. 2K exhibits negligible changes in conformation in the presence of liposomes. 3K in PBS also retains its spectral pattern however in water, a change in conformation is observed only in the case of PC. EEK behaves almost similar to 3K, with the exception of demonstrating no significant changes in conformation in presence of both PC and PC/PG in PBS. The peptide concentration was 125 μM and the ratio of peptide : liposome was maintained at 1 : 10. Note the relative intensities on the *y* axis are different for better visibility of the individual structural changes.

perturb the acyl chain region of the lipids (Fig. S9d, S11d and S12d, ESI†). These IR spectra confirm that all peptides interact with the lipid bilayers, however, their assembled state affects initial depth of insertion, and for higher oligomers most likely a surface coverage occurs initially, similar to carpet mechanism[57–59] (for more details see Fig. S9–S12 and related text in ESI†). Note, that the above shifts experienced for symmetric and asymmetric vibrations[60,61] could result from deep insertion into the bilayer[56] or from inducing the perturbation of the lipid packing, while remaining on the surface of the membrane, as seen with certain AMPs.[59,62]

To determine the size of the molecular aggregates formed, DLS measurements were also performed. The size of untreated liposomes was maintained at ~100 nm for the PC and PC/PG vesicles (Fig. S8 and Table S2, ESI†). The size distribution of peptides in PBS without liposomes revealed molecular associates in the micrometer range, while in water, the peptides alone exhibited 70 nm to 200 nm assemblies. Interestingly, when the peptides were added to liposomes, the monodisperse size distribution became polydisperse, with an indication of the formation of aggregates (Fig. S8 and Table S2, ESI†).

Besides, the polydispersity index (PdI) from DLS provides further information about the heterogeneity of the liposome systems. EKK-H_2O and 3K-H_2O upon addition to liposomes exhibit a radical increase from a monodisperse state to a polydisperse state *e.g.* with a PdI of ~ 0.6 for PC (Table S2, ESI†). In contrast, adding 2K-H_2O to liposomes provide a monodisperse state for both PC and PC/PG and the same applies to EK-H_2O both for PC and PC/PG with an index of ~0.3.

In PBS, when the three peptides EK, 2K, and 3K, were added to PC and PC/PG, the system became monodisperse, in contrast to the hyperdispersed samples of the peptides alone (PdI ~ 0.7). At the same time, EKK remained highly polydisperse in PC/PG in PBS media (Table S2, ESI†).

Additionally, we also measured zeta potential, which is a key indicator of colloidal stability and provides insights to membrane interactions, especially on the solution-bilayer interface.[63–65] As mentioned above, in contrast to the three peptides (EK, 2K, and 3K), which reached a monodisperse solution when interacting with liposomes, EKK remained an exception with a high polydispersity in the presence of PC/PG liposomes in PBS media (Table S2, ESI†). Therefore, we focused on EKK in comparison with 3K (Table S3, ESI†). The zeta potential of the control, PC in water was −34.5 mV. The addition of 3K resulted in a significant increase to −17 mV. In contrast, EKK-H_2O-PC showed no significant change (−32.5 mV). In case of negatively charged liposomes, PC/PG in water, the zeta potential was observed to be −66.4 mV and upon addition of EKK and 3K, there was a slight increase to ~−51 mV. In PBS, the zeta potential of control PC was recorded to be −27.3 mV. This value was not substantially affected by EKK or 3K, possibly due to the preformed structures not affecting the surrounding region of the liposome. In PBS, PC/PG control exhibited a zeta potential of −65 mV. Here the complex 3K-PBS-PC/PG showed a decrease in the value to −85.9 mV, while EKK-PBS-PC/PG showed a slight increase to −48.4 mV. Note that these β-peptide supramolecular systems have not been tested thus far by zeta potential measurements in the presence of liposomes, thus for qualitative comparison, the liposomes were also evaluated with well-characterized

cationic antimicrobial peptides with charges ranging from 0 to +6 (see text in ESI† and Table S4), which we have also addressed extensively in similar setups.[66] Based on these, the above values fit in the range of the natural systems, and display similar qualitative observations when relative comparisons between treated and non-treated lipid systems were considered.

Hemolytic activity

To support the above observations with more complex biomembranes, and analyze the preliminary cytotoxicity of these peptides, we have supplemented the liposome studies with eukaryotic membranes *via* hemolysis assays. The membrane of human erythrocytes is composed of proteins, lipids and glycoproteins and is often used for studying membrane perturbation effects.[67] In PBS, hemolysis assays revealed that 3K had the highest hemolytic activity with a HC_{50} value of ~30 μM followed by EK and 2K (with HC_{50} = 92 μM and HC_{50} = 103 μM respectively). EKK had the lowest hemolytic activity among the four peptides with an estimated HC_{50} of more than 250 μM (Fig. 4 and Table S5, ESI†). It should be noted that the difference between the HC_{50} values of 3K and EKK was significant, more than an order of magnitude, while EK and 2K showed almost equal hemolytic activity. Interestingly, these observations contradict previous conclusions correlating hydrophobicity and hemolytic activity to some extent.[68] Here, the highest hemolytic activity is shown by 3K which is the most cationic. This can be attributed to the lamellar supramolecular form that is prevalent in PBS media, which could drastically affect the overall membrane disrupting affinity. However, the significant difference in hemolytic activity resulting to approximately one order of magnitude upon slight sequential modifications is indicative of the dependence of peptide sequence on such activites. These findings provide a promising platform for further modifications and show that these peptides can have both benign and toxic effect on human cells that can be further developed towards specific needs in biomedicine. In this regard, single Glu side chain insertions could be foreseen, which may reduce toxic effects while retaining supramolecular assembly formation. Nevertheless, more in-depth studies are needed in this direction to carefully assess the effect of specific residues and side chains on hemolytic activity.

Overview on Surface affinity

To decipher how the presence of membrane could alter the macromolecular morphologies, DLS measurements, zeta potential measurements, CD and IR spectra, and TEM images were used in combination to identify major changes.

In water, the 3K-H_2O-PC complex led to a notable rise in zeta potential, and a drastic increase in the PdI. These indicate a transition from a monodisperse ~100 nm liposome system to an unstable polydisperse solution. CD measurements corroborated with these observations and for 3K upon adding PC liposomes, a significant change occurred from random coil 3K-H_2O towards a more ordered CD signal in the 3K-H_2O-PC system (Fig. 3(d)). This would suggest that 3K interacts with PC liposomes, although likely some 3K aggregates will also be formed in the solution, resulting in a polydisperse system.

In contrast, EKK when added to PC in water showed no significant change in the zeta potential value which is in accordance with the CD spectra that showed minor variations along with the IR spectra where no substantial perturbation can be observed in the three regions associated to the lipid moieties (Fig. 3(b), Fig. S9d, f and Table S3, ESI†). However, the DLS measurements demonstrate a significant increase in polydispersity, which is presumably due to the preformed structure of EKK in water as observed in the TEM images (Fig. 2(c) and Table S2, ESI†). Here, these overall results suggest that EKK-H_2O alone forms supramolecules, and these will be retained even in presence of PC, but there is practically no interaction between the EKK assemblies and PC liposomes.

In case of PC/PG in water, upon addition of 3K, there was a slight increase in zeta potential values when compared to the liposome alone (Table S3, ESI†). For 3K-H_2O-PC/PG, DLS measurements indicate a similar monodispersed solution as

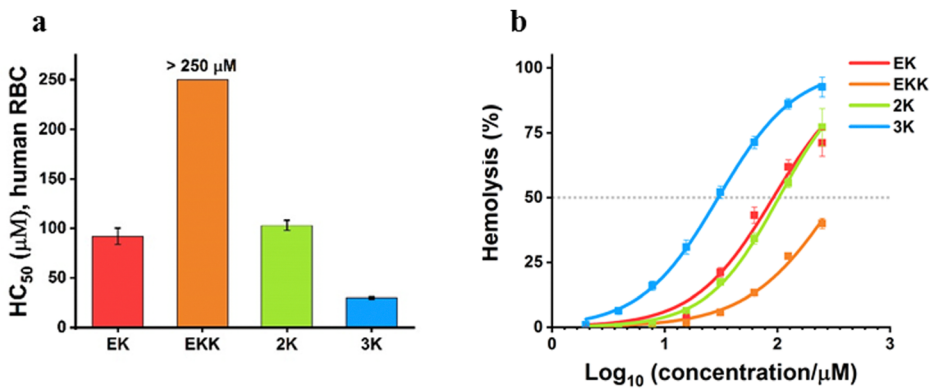

Fig. 4 Hemolytic activity of the peptides tested on human red blood cells in PBS. (a) The half-maximal hemolysis concentration (HC_{50}) values of the peptides. Peptides were tested on human red blood cells (1% (V/V)) and based on the dose–response curves after fitting with non-linear regression on the hemolysis percentage, HC_{50} values were determined. Bars represent mean ± SD, N = 4, (b) Hemolytic activity of the peptides. The percentage of hemolysis, compared to PBS-treated RBC as negative control, was plotted. As positive control, the bee-venom melittin was applied at 10 μM concentration. Data are presented as mean ± SD (N = 4).

observed for 3K-H_2O alone. Interestingly, this is contrasted by 3K-H_2O-PC, where the PdI increased and the negative zeta potential decreased markedly (Tables S2 and S3, ESI†). Also, the CD spectrum displays no indication of 3K assembly formation (Fig. 3(d)). This difference in behaviour could be attributed to the electrostatic interactions between the monomeric 3K molecules and the negatively charged PC/PG liposomes. It was earlier demonstrated that in equilibrium, 3K samples have monomers,[36] as it could be that PC/PG liposomes prefer these cationic molecules, likely causing partial disassembly of larger aggregates by ''dissolving'' the monomers in the lipid bilayer region. Thus, here we conclude that 3K in water interacts with PC/PG, but in monomeric form.

EKK-H_2O-PC/PG showed a somewhat higher polydispersity, although the zeta potential, and the CD spectra showed close similarity to that of 3K-H_2O-PC/PG (Fig. 3(b), (d), Tables S2 and S3, ESI†). IR data showed that both peptides interact with the lipid molecules (Fig. S9 and S12, ESI†), though the +3 charged 3K perturbs the phosphate vibrations, indicating localization in the headgroup region, whereas +1 charged EKK caused shift in the symmetric and asymmetric vibrations of the CH_2 groups, thus EKK likely resides in the acyl chain area of the PC/PG bilayer. Most probably its hydrophobic domain will be more dominant here, which is also supported by its increased binding capacity with ANS (Fig. S1, ESI†). Based on this, we approximate that EKK also binds to PC/PG mainly in a monomeric form. Furthermore, while 3K prefers the headgroup region, EKK likely inserts into the acyl chain region of the bilayer.

The zeta potential of the zwitterionic liposome PC in PBS is quite similar to EKK-PBS-PC and 3K-PBS-PC, as a certain degree of stabilization is attained, indicated by the PdI (Tables S2 and S3, ESI†). Additionally, CD and IR results substantiate that there is no significant effect on liposomes. This is attributed to the lamellin formation of 3K and EKK in PBS, which hinders any perturbation of the lipid membrane due to the presence of the superstructure (Fig. 3(b), (d), Fig. S9 and S12, ESI†). In the case of EKK, this is further confirmed by the haemolytic tests, where the PC liposome in PBS system, is a comparable model of the human red blood cells, displaying a high HC_{50} values (Fig. 4 and ESI,† Table S5). Note, that the monodispersity nature of the 3K-PBS-PC system, as opposed to 3K-PBS alone, suggests that for this peptide there could be some sort of peptide-liposome interaction, which is also supported by the haemolytic toxicity for 3K. However, the nature of this interaction cannot be satisfactorily identified at this point.

Intriguingly, for 3K-PBS-PC/PG both DLS and zeta potential values suggest a stable, monodisperse system (Tables S1 and S2, ESI†). It was recently demonstrated that, in equilibrium, 3K-PBS samples contain monomers and assemblies as well,[36] possibly leading the affinity between PC/PG liposomes and the 3K molecules. The partial disassembly of larger supramolecules can also be seen in the reduced intensity of the CD signal (Fig. 3(d)). In overall, it seems that 3K in PBS definitely interacts with PC/PG likely in both supramolecular and monomeric forms.

In contrast, the PdI of EKK-PBS-PC/PG is higher, while the zeta potential increases compared to that of PC/PG in PBS (Tables S2 and S3, ESI†). This is accompanied with a similar reduced CD signal of EKK lamellae (Fig. 3(b)), hence, considering its lower charge, it is assumed that EKK in PBS interacts with PC/PG, but to a lower extent as 3K and also, based on the increase in PdI values it will have a higher proportion remaining in the macromolecular form.

Regarding the two other peptides, for EK in water, DLS mass distribution reveals two populations, consistent with the TEM observations of long twisted fibrils and short assemblies (Fig. 2(a), Fig. S7, Tables S1 and S2, ESI†). Surprisingly, in the presence of PC and PC/PG liposomes in water, a single population with a PdI of $\sim$0.3 is observed, reflecting uniformity in the EK-liposome complex. This finding aligns with the CD spectral patterns and IR data, indicating interactions with the lipid bilayer in both the acyl chain and phosphate regions (Fig. 3(a) and Fig. S10, ESI†).

When 2K in water is added to PC and PC/PG liposomes, no drastic changes in the CD spectra are observed (Fig. 3(c)). However, slight perturbations in the phosphate region of the IR spectra are seen, which can be attributed to the surface localization of the monomeric 2K, similar to what is observed with 3K[36] (Fig. S11, ESI†). Note that, although EK-PBS-PC and 2K-PBS-PC display distinct CD spectra and do not produce comparable spectroscopic results, they exhibit similar behavior in DLS by reducing their polydispersity, leading to a more uniform peptide–PBS–PC complex. This similarity along with their comparable sequence length, may contribute to their similar HC_{50} values.

In overall, although there are notable differences, all four peptides show membrane activity, akin to the previous lamellin β-peptides.[35] Based on earlier studies, where we focused on lipid interactions and assembly formation of some of these compounds using also molecular dynamics simulations,[35,36] we can assume several common features for lamellins. In water their assembly formation is driven primarily by the formation of the hydrophobic Leu core, which can be strengthened by the coordination capacity of ions present in the media, given the right charged side chains are present, such as lysines here. Once in a membrane environment, the hydrophobic core has affinity to be either adsorbed on the lipid bilayer or be even incorporated deeper into the acyl chain region. The results presented above clearly demonstrate that these basic scenarios can be significantly altered by the sequential modifications, reaching to the unique characteristics for the four studied peptides. However, the detailed understanding of their particular differences would require further extensive theoretical and experimental investigations, a direction that is beyond our current scope.

Conclusion

Here, we have investigated the assembly formation characteristics and the membrane affinity of four lamellin β-peptides with varying charge and length in both aqueous and physiological PBS media using various biophysical characterization

techniques. Higher assembling propensity was observed for the octapeptides as indicated by the occurrence of the characteristic 205 nm CD spectral maximum of lamellins. The assembly formation was also more pronounced in PBS medium owing to the electrostatic interactions arising from the charged constructs as evidenced by the presence of structured lamellar patterns for both EKK and EK observed in the TEM images. Structural assays on lipid membrane interaction indicate that the peptides maintain their secondary structure while they likely fold around the liposomes to form an uniform supramolecular assembly without disassembly of the lamellae. Moreover, the peptides demonstrate varying degrees of hemolytic activity suggesting that their structure and assembling properties play a major role in modulating their toxicity. Note that lamellins are a unique addition to the previous set of β-peptide antimicrobials, as these seem to reach antimicrobial activity from a macromolecular direction. Their toxic effect on bacterial membranes is initiated by lethal assembly formation on the target surfaces. However, the applicability of these novel compounds to form layered templates potentially points well beyond specific areas. Overall, this study provides an insight into the crucial interplay between noncovalent and solvent interactions of these lamellin β-peptide assemblies which can be manipulated by effective control over charge and length to engineer functional bioactive supramolecules for biomedical applications.

Methods

Peptide synthesis

Solid-phase peptide synthesis of the peptides was carried out in a continuous flow reactor.[69] The coupling reagents and solvents used for the synthesis, such as 1,8-diazabicyclo[5.4.0]undec-7-ene (DBU), piperidine, trifluoroacetic acid (TFA), *N*,*N*-dimethylformamide (DMF), 1-[bis(dimethylamino)methylene]-1*H*-1,2,3-triazolo[4,5-*b*]-pyridinium-3-oxide hexafluorophosphate (HATU) and *N*,*N*-diisopropylethylamine (DIPEA) were purchased from Merck Life Science (Budapest, Hungary). TentaGel R RAM resin (capacity = 0.19 mmol g^{-1}), purchased from Rapp Polymere GmbH, was loaded into the column (125 × 4 mm). Fmoc-protected amino acid (2.5 equiv.), HATU (2.5 equiv.) and DIPEA (5 equiv.) were dissolved in 1.5 mL of DMF for the coupling. The flow rate was adjusted to 0.15 mL min^{-1} while the pressure and temperature were maintained at 60 bar and 70 °C respectively. 2% DBU and 2% piperidine in DMF were used for Fmoc-deprotection. After coupling and deprotection, the resin was washed with DMF. The peptides were then cleaved by stirring for 3 h in a solution of 95% TFA and 5% water. After evaporation of the TFA, the peptides were precipitated in cold diethyl ether. The crude peptides were purified by reversed-phase HPLC followed by lyophilization. The peptides were analyzed on an LC-40 HPLC system (Shimadzu, Kyoto, Japan) on a Phenomenex Jupiter Proteo C12 column (10 μm, 90 Å, 4.6 mm × 150 mm) using gradient elution with eluent A (0.1% TFA in H_2O) and eluent B (0.1% TFA in ACN : H_2O = 80 : 20 (v/v)). The flow rate was 1 mL min^{-1}, the gradient was 5–100 B% in 20 min (UV detection at λ = 214 nm). High-resolution mass spectrometry was performed on a Q Exactive Plus Hybrid Quadrupole-Orbitrap Mass Spectrometer (Thermo Scientific, Waltham, MA, USA). Monoisotopic molecular mass for EK [$C_{45}H_{84}N_8O_9$] calculated = 880.6361, observed = 880.6335; EKK [$C_{58}H_{109}N_{11}O_{11}$] calculated = 1135.8308, observed = 1135.8278; 2K [$C_{46}H_{89}N_9O_7$] calculated = 879.6885, observed = 879.6862; 3K [$C_{60}H_{116}N_{12}O_9$] calculated = 1148.8988, observed = 1148.8954 (Fig. S13–S16). In all cases, the measured mass was within 3 ppm of the accurate mass.

Preparation of peptide solutions

The peptides were tested in pure MQ water and phosphate buffered saline (PBS). For preparation of the peptide solutions, 125 μM of the peptide was used: in H_2O, pH 6.5, sonicated for 10 min and in 10 mM PBS (137 mM NaCl, 2.7 mM KCl, 10 mM of disodium hydrogen phosphate, 2 mM of sodium dihydrogen phosphate), pH 7.4, sonicated for 30 min at 25 °C. The co-assemblies were formed immediately upon sonication and their structural configuration was tested using CD spectroscopy. Upon re-investigation with the same method after 24 hours, similar spectral patterns were observed in the CD indicating no further assembly formation.

Preparation of liposomes

High purity synthetic 1,2-dioleoyl-*sn-glycero*-3-phosphocholine (DOPC) and 1,2-dioleoyl-*sn-glycero*-3-[phospho-*rac*-(1-glycerol)], sodium salt (DOPG) was purchased from NOF (Tokyo, Japan). Liposomes were prepared by using the lipid thin film hydration technique. Lipids were dissolved in chloroform (LabScan, Budapest, Hungary) containing 50 vol% methanol (Reanal, Budapest, Hungary), which was then evaporated using a rotary evaporator. The resulting lipid film was kept in vacuum for at least 8h to remove residual traces of solvent. The dried lipid film was hydrated with the assay buffer. After repeated heating (37 °C) and cooling (−196 °C) steps, the solutions were extruded through polycarbonate filters of 100 nm pore size (at least 11 times) using a LIPEX extruder (Northern Lipids Inc., Burnaby, Canada). The stock solution was prepared at 13 mM which was diluted 10 times for all measurements with the corresponding medium. For mimicking basic properties of mammalian and bacterial cell membranes, pure DOPC and DOPC/DOPG (80/20 n/n%), were used throughout the study.

Circular dichroism (CD) spectroscopy

CD spectra were collected at room temperature using a JASCO J-1500 spectropolarimeter (JASCO, Tokyo, Japan). A rectangular quartz cuvette with a 0.1 cm path length (Hellma, Plainview, NY) was used in continuous mode between 190 nm to 260 nm with a scanning speed of 50 nm min^{-1}, a data pitch of 0.5 nm, response time of 4 s, bandwidth of 2 nm and 3 accumulations. 125 μM of the peptides (200 μL) were used. For the artificial model membranes, a concentration ratio of peptide-to-liposome of 1 : 10 was prepared. All the spectra were corrected by subtracting a corresponding/matching blank.

Attenuated total reflection-Fourier transform infrared (ATR-FTIR) spectroscopy

FTIR spectroscopic measurements were performed using a Varian 2000 FTIR Scimitar spectrometer equipped with a Golden Gate accessory (Varian Inc., Palo Alto, CA). 3 μL of the peptides in the aforementioned concentration were pipetted onto the diamond ATR surface and the solvent was evaporated under ambient conditions to obtain a dry film. The spectra were collected at 2 cm^{-1} nominal resolution applying 64 scans. Data acquisition was followed by ATR correction, baseline correction and buffer subtraction. All spectral manipulations were performed using the GRAMS/32 software package (Galactic Inc, USA).

Fluorescence spectroscopy

Fluorescence spectra were recorded using a JASCO FP-8500 spectrofluorometer with an excitation and emission bandwidth of 10 nm and 20 nm, respectively. Three accumulations were measured each time. The 8-anilino-1-naphthalenesulfonic acid (ANS) fluorophore was excited at 388 nm and the emission was recorded from 410 to 600 nm. Binding assays were performed using 125 μM peptide (50 μL) and 2.5 μM ANS. Spectra were corrected for those of the corresponding peptide solutions.

Transmission electron microscopy

2 μL of the samples were pipetted in each case to a 200-mesh copper grid (Ted Pella, Inc, California, USA) with a support film made of formvar. After a contact time of 1 min, excess liquid was removed, and samples were stained with 2% of uranyl acetate. TEM images were obtained routinely at magnifications of 11 000×, 28 000×, 71 000× and 180 000× using a Morgagni 268D (FEI, The Netherlands) operating at 80 kV.

Dynamic light scattering (DLS)

Particle size and size distribution of the peptides and the mixture peptide-liposome were measured with a W130i dynamic light scattering device (DLS, Avid Nano, Ltd, High Wycombe, UK) with a diode laser (660 nm) and a photodiode detector, using low-volume disposable cuvettes with 1 cm path length (UVette, Eppendorf, Vienna, Austria, GmbH) and a final sample volume of 80 μL at 20 °C. 125 μM of the peptides (80 μL) were used. For the artificial model membranes, a concentration ratio of peptide-to-liposome of 1 : 10 was prepared. The time-dependent autocorrelation functions were measured for 10 s, repeated 10 times and averaged. Data analysis reaching the mean hydrodynamic diameter and polydispersity were performed with the iSize 3.0 software supplied with the device.

Zeta potential measurement

A Zetasizer Nano ZS (Malvern Panalytical GmbH, Germany) with disposable folded capillary cells was used to determine the zeta-potential (ζ-potential) of the liposomes prepared in water or 1× PBS and peptide (EKK and 3K) treated liposome samples. Known AMPs such as p53 (17–26), aurein 1.2, dermicidin and CM15 were prepared in water and in PBS to reach 125 μM. A concentration ratio of peptide-to-liposome of 1 : 10 was maintained for model membranes. Each sample (100 μL) was diluted with 700 μL of water. The initial samples were prepared in PBS (1×, containing 137 mM NaCl and 2.7 mM KCl, pH 7.4) and then diluted eight-fold, resulting in a final solution with a PBS concentration of 0.125×. The measurement was performed at 25 °C after 3 min of equilibration. Each measurement was repeated in triplicate and mean values, as well as standard deviations, were calculated.

Hemolysis assay

Hemolytic activity of the peptides was tested on human red blood cells (RBC), obtained from the Hungarian National Blood Transfusion Service (Budapest, Hungary). First, RBCs were washed twice with PBS, then diluted with PBS (2% V/V) and plated on a 96-well, round-bottom plate (Sarstedt, Nümbrecht, Germany) at a volume of 50 μL. Serial dilution of the peptides were prepared, starting from 500 μM concentration, and added to the wells at a volume of 50 μL. The final RBC concentrate was 1% V/V, and the final volume was 100 μL in the wells. Plates were incubated at 37 °C, 5% CO_2 for 2 h, centrifuged at 2000 rpm (5 min, 4 °C) and then 50 μL of the supernatants were carefully transferred to a new plate, containing 100 μL H_2O in each well. Optical density (OD) was measured at 414 and 450 nm by a Synergy 2 multimode microplate reader (BioTek, Winooski, VT, USA) and the percentage of hemolysis, compared to a well-known hemolytic peptide, namely the bee venom Melittin (10 μM), was determined. All data presented as the mean ± SD, (N = 4). The half-maximal hemolysis concentration (HC_{50}) values were calculated from the dose–response curves after fitting with non-linear regression.

Statistical analysis and reproducibility

All the data are expressed as mean ± standard deviation. The CD, IR and Fluorescence spectroscopy measurements were performed in triplicates for three independent sets of experiments. For hemolysis assay, data presented are as the mean ± standard deviation (N = 4).

Author contributions

Sohini Chakraborty: conceptualization, data curation, investigation, methodology, validation, visualization, writing – original draft, writing – review & editing. Kamal el Battioui: conceptualization, data curation, investigation, methodology, validation, visualization, writing – original draft, writing – review & editing. Tasvilla Sonallya: investigation, methodology, validation. Imola Cs. Szigyártó: investigation, validation, Kata Horváti: investigation, methodology, resources, validation. Zoltán Varga: investigation, resources, validation. Tünde Juhász: investigation, methodology, validation, writing – review & editing. Tamás Beke-Somfai: conceptualization, funding acquisition, project administration, resources, supervision, validation, writing – review & editing.

Data availability

The authors confirm that the data supporting the findings of this study are available within the article and its ESI.†

Conflicts of interest

There are no conflicts to declare.

Acknowledgements

This work was funded by the National Research, Development and Innovation Office, Hungary (TKP2021-EGA-31, 2020-1.1.2-PIACI-KFI-2020-00021 and KKP_22 Ppoject no. 144180). Support from Eötvös Loránd Research Network, grant no. SA-87/2021 and KEP-5/2021 are also acknowledged.

References

1 J. P. S. Powers and R. E. W. Hancock, *Peptides*, 2003, **24**, 1681–1691.
2 J. Y. Rho, H. Cox, E. D. H. Mansfield, S. H. Ellacott, R. Peltier, J. C. Brendel, M. Hartlieb, T. A. Waigh and S. Perrier, *Nat. Commun.*, 2019, **10**, 4708–4716.
3 N. Habibi, N. Kamaly, A. Memic and H. Shafiee, *Nano Today*, 2016, **11**, 41–60.
4 N. P. King, J. B. Bale, W. Sheffler, D. E. McNamara, S. Gonen, T. Gonen, T. O. Yeates and D. Baker, *Nature*, 2014, **510**, 103–108.
5 T. Yu, O.-S. Lee and G. C. Schatz, *J. Phys. Chem. A*, 2014, **118**, 8553–8562.
6 S. E. Paramonov, H. W. Jun and J. D. Hartgerink, *J. Am. Chem. Soc.*, 2006, **128**, 7291–7298.
7 R. Pugliese, *Biophysica*, 2022, **2**, 324–339.
8 E. Gazit, *FASEB J.*, 2002, **16**, 77–83.
9 B. Nizami, D. Bereczki-Szakál, N. Varró, K. El Battioui, V. U. Nagaraj, I. C. Szigyártó, I. Mándity and T. Beke-Somfai, *Nucleic Acids Res.*, 2020, **48**, D1122–D1128.
10 H. Zhu, H. Wang, B. Shi, L. Shangguan, W. Tong, G. Yu, Z. Mao and F. Huang, *Nat. Commun.*, 2019, **10**, 1–10.
11 A. W. Simonson, M. R. Aronson, S. H. Medina and S. H. Medina, *Molecules*, 2020, **25**, 2751.
12 S. Chakraborty, K. el Battioui and T. Beke-Somfai, *Small Sci.*, 2024, **4**, 2300217.
13 Y. H. No, N. H. Kim, B. Gnapareddy, B. Choi, Y.-T. Kim, S. R. Dugasani, O.-S. Lee, K.-H. Kim, Y.-S. Ko, S. Lee, S. W. Lee, S. H. Park, K. Eom and Y. H. Kim, *J. Phys. Chem. Lett.*, 2017, **8**, 3734–3739.
14 H.-S. Jang, J.-H. Lee, Y.-S. Park, Y.-O. Kim, J. Park, T.-Y. Yang, K. Jin, J. Lee, S. Park, J. M. You, K.-W. Jeong, A. Shin, I.-S. Oh, M.-K. Kwon, Y.-I. Kim, H.-H. Cho, H. N. Han, Y. Kim, Y. H. Chang, S. R. Paik, K. T. Nam and Y.-S. Lee, *Nat. Commun.*, 2014, **5**, 3665.
15 D. Mandal, A. Nasrolahi Shirazi and K. Parang, *Org. Biomol. Chem.*, 2014, **12**, 3544–3561.
16 D. Seebach, S. Abele, J. V. Schreiber, B. Martinoni, A. K. Nussbaum, H. Schild, H. Schulz, H. Hennecke, R. Woessner and F. Bitsch, *Chimia*, 1998, **52**, 734.
17 H. Chu, M. Pazgier, G. Jung, S. P. Nuccio, P. A. Castillo, M. F. De Jong, M. G. Winter, S. E. Winter, J. Wehkamp, B. Shen, N. H. Salzman, M. A. Underwood, R. M. Tsolis, G. M. Young, W. Lu, R. I. Lehrer, A. J. Bäumler and C. L. Bevins, *Science*, 2012, **337**, 477–481.
18 P. S. P. Wang and A. Schepartz, *Chem. Commun.*, 2016, **52**, 7420–7432.
19 G. Pohl, T. Beke-Somfai, I. G. Csizmadia and A. Perczel, *Amino Acids*, 2012, **43**, 735–749.
20 A. Wacha, Z. Varga and T. Beke-Somfai, *J. Chem. Inf. Model.*, 2023, **63**, 3799–3813.
21 P. G. Vasudev, S. Chatterjee, S. Narayanaswamy and B. Padmanabhan, *Chem. Rev.*, 2011, **111**, 657–687.
22 D. Seebach, A. K. Beck and D. J. Bierbaum, *Chem. Biodiversity*, 2004, **1**, 1111–1239.
23 T. A. Martinek, I. M. Mándity, L. Fülöp, G. K. Tóth, E. Vass, M. Hollósi, E. Forró and F. Fülöp, *J. Am. Chem. Soc.*, 2006, **128**, 13539–13544.
24 A. Szloszár, F. Fülöp and I. M. Mándity, *ChemistrySelect*, 2017, **2**, 6036–6039.
25 D. Liu and W. F. DeGrado, *J. Am. Chem. Soc.*, 2001, **123**, 7553–7559.
26 Y. Hamuro, J. P. Schneider and W. F. DeGrado, *J. Am. Chem. Soc.*, 1999, **121**, 12200–12201.
27 P. I. Arvidsson, J. Frackenpohl, N. S. Ryder, B. Liechty, F. Petersen, H. Zimmermann, G. P. Camenisch, R. Woessner and D. Seebach, *ChemBioChem*, 2001, **2**, 771–773.
28 B. Bozü, F. Fülöp, G. K. Tóth, G. Tóth and M. Szücs, *Neuropeptides*, 1997, **31**, 367–372.
29 D. Seebach and J. Gardiner, *Acc. Chem. Res.*, 2008, **41**, 1366–1375.
30 P. C. Ke, R. Zhou, L. C. Serpell, R. Riek, T. P. J. Knowles, H. A. Lashuel, E. Gazit, I. W. Hamley, T. P. Davis, M. Fändrich, D. E. Otzen, M. R. Chapman, C. M. Dobson, D. S. Eisenberg and R. Mezzenga, *Chem. Soc. Rev.*, 2020, **49**, 5473–5509.
31 E. A. Porter, B. Weisblum and S. H. Gellman, *J. Am. Chem. Soc.*, 2002, **124**, 7324–7330.
32 M. Zasloff, *Proc. Natl. Acad. Sci. U. S. A.*, 1987, **84**, 5449–5453.
33 P. I. Arvidsson, N. S. Ryder, H. M. Weiss, G. Gross, O. Kretz, R. Woessner and D. Seebach, *ChemBioChem*, 2003, **4**, 1345–1347.
34 S. Mosca, J. Keller, N. Azzouz, S. Wagner, A. Titz, P. H. Seeberger, G. Brezesinski and L. Hartmann, *Biomacromolecules*, 2014, **15**, 1687–1695.
35 I. C. Szigyártó, J. Mihály, A. Wacha, D. Bogdán, T. Juhász, G. Kohut, G. Schlosser, F. Zsila, V. Urlacher, Z. Varga, F. Fülöp, A. Bóta, I. Mándity and T. Beke-Somfai, *Chem. Sci.*, 2020, **11**, 6868–6881.
36 K. el Battioui, S. Chakraborty, A. Wacha, D. Molnár, M. Quemé-Peña, I. C. Szigyártó, C. L. Szabó, A. Bodor, K. Horváti, G. Gyulai, S. Bősze, J. Mihály, B. Jezsó, L. Románszki, J. Tóth, Z. Varga, I. Mándity, T. Juhász and T. Beke-Somfai, *Nat. Commun.*, 2024, **15**, 3424.

37 S. Li, Y. Wang, Z. Xue, Y. Jia, R. Li, C. He and H. Chen, *Trends Food Sci. Technol.*, 2021, **109**, 103–115.
38 M. G. Ciulla and F. Gelain, *Microb. Biotechnol.*, 2023, **16**, 757–777.
39 B. Nordén, A. Rodger and T. Dafforn, *Linear dichroism and circular dichroism: a textbook on polarized-light spectroscopy*, 2010.
40 A. Glättli, X. Daura, D. Seebach and W. F. Van Gunsteren, *J. Am. Chem. Soc.*, 2002, **124**, 12972–12978.
41 D. Seebach, J. V. Schreiber, P. I. Arvidsson and J. Frackenpohl, *Helv. Chim. Acta*, 2001, **84**, 271–279.
42 T. A. Martinek, G. K. Tóth, E. Vass, M. Hollósi and F. Fülöp, *Angew. Chem., Int. Ed.*, 2002, **41**, 1718–1721.
43 A. Micsonai, F. Wien, L. Kernya, Y. H. Lee, Y. Goto, M. Réfrégiers and J. Kardos, *Proc. Natl. Acad. Sci. U. S. A.*, 2015, **112**, E3095–E3103.
44 T. Beke, C. Somlai, G. Magyarfalvi, A. Perczel and G. Tarczay, *J. Phys. Chem. B*, 2009, **113**, 7918–7926.
45 W. H. James, E. E. Baquero, V. A. Shubert, S. H. Choi, S. H. Gellman and T. S. Zwier, *J. Am. Chem. Soc.*, 2009, **131**, 6574–6590.
46 A. Barth, *Biochim. Biophys. Acta, Bioenerg.*, 2007, **1767**, 1073–1101.
47 A. Hetényi, I. M. Mándity, T. A. Martinek, G. K. Tóth and F. Fülöp, *J. Am. Chem. Soc.*, 2005, **127**, 547–553.
48 G. Montalvo, M. M. Waegele, S. Shandler, F. Gai and W. F. DeGrado, *J. Am. Chem. Soc.*, 2010, **132**, 5616–5618.
49 A. M. Petrosyan and V. V. Ghazaryan, *J. Mol. Struct.*, 2009, **917**, 56–62.
50 H. Meuzelaar, J. Vreede and S. Woutersen, *Biophys. J.*, 2016, **110**, 2328–2341.
51 C. A. Royer, *Chem. Rev.*, 2006, **106**, 1769–1784.
52 A. Hawe, M. Sutter and W. Jiskoot, *Pharm. Res.*, 2008, **25**, 1487–1499.
53 V. Vetri, C. Canale, A. Relini, F. Librizzi, V. Militello, A. Gliozzi and M. Leone, *Biophys. Chem.*, 2007, **125**, 184–190.
54 D. Willbold, B. Strodel, G. F. Schröder, W. Hoyer and H. Heise, *Chem. Rev.*, 2021, **121**, 8285–8307.
55 L. K. Tamm and S. A. Tatulian, *Q. Rev. Biophys.*, 1997, **30**, 365–429.
56 R. N. A. H. Lewis, E. J. Prenner, L. H. Kondejewski, C. R. Flach, R. Mendelsohn, R. S. Hodges and R. N. McElhaney, *Biochemistry*, 1999, **38**, 15193–15203.
57 J. W. Brauner, R. Mendelsohn and F. G. Prendergast, *Biochemistry*, 1987, **26**, 8151–8158.
58 M. Quemé-Peña, T. Juhász, J. Mihály, I. Cs Szigyártó, K. Horváti, S. Bősze, J. Henczkó, B. Pályi, C. Németh, Z. Varga, F. Zsila and T. Beke-Somfai, *ChemBioChem*, 2019, **20**, 1578–1590.
59 M. Quemé-peña, T. Juhász, G. Kohut, M. Ricci, P. Singh, I. C. Szigyártó, Z. I. Papp, L. Fülöp and T. Beke-somfai, *Int. J. Mol. Sci.*, 2021, **22**, 8613.
60 S. Castano and B. Desbat, *Biochim. Biophys. Acta, Biomembr.*, 2005, **1715**, 81–95.
61 R. N. A. H. Lewis and R. N. McElhaney, *Biochim. Biophys. Acta, Biomembr.*, 2013, **1828**, 2347–2358.
62 T. Juhász, M. Quemé-Peña, B. Kővágó, J. Mihály, M. Ricci, K. Horváti, S. Bősze, F. Zsila and T. Beke-Somfai, *Sci. Rep.*, 2021, **11**, 1–15.
63 S. Samimi, N. Maghsoudnia, R. B. Eftekhari and F. Dorkoosh, *Lipid-Based Nanoparticles for Drug Delivery Systems*, Elsevier Inc., 2018.
64 M. C. Smith, R. M. Crist, J. D. Clogston and S. E. McNeil, *Anal. Bioanal. Chem.*, 2017, **409**, 5779–5787.
65 Z. Németh, I. Csóka, R. Semnani Jazani, B. Sipos, H. Haspel, G. Kozma, Z. Kónya and D. G. Dobó, *Pharmaceutics*, 2022, **14**, 1798.
66 T. Sonallya, T. Juhász, I. C. Szigyártó, K. Ilyés, P. Singh, D. Khamari, E. I. Buzás, Z. Varga and T. Beke-Somfai, *J. Colloid Interface Sci.*, 2025, **679**, 496–509.
67 I. Greco, N. Molchanova, E. Holmedal, H. Jenssen, B. D. Hummel, J. L. Watts, J. Håkansson, P. R. Hansen and J. Svenson, *Sci. Rep.*, 2020, **10**, 1–13.
68 K. Kuroda, G. A. Caputo and W. F. DeGrado, *Chem. – Eur. J.*, 2009, **15**, 1123–1133.
69 I. Nekkaa, D. Bogdán, T. Gáti, S. Béni, T. Juhász, M. Palkó, G. Paragi, G. K. Tóth, F. Fülöp and I. M. Mándity, *Chem. Commun.*, 2019, **55**, 3061–3064.